POLITECNICO DI TORINO
Repository ISTITUZIONALE

Sonic Boom Numerical Validation of a Mach 4.7 Experimental Test

Original
Sonic Boom Numerical Validation of a Mach 4.7 Experimental Test / Graziani, S., Viola, N., Fusaro, R., Hengy, S., Albisser, M., Martinez, B.. - (2024). (30th AIAA/CEAS Aeroacoustics Conference (2024) Roma (ITA) June 4-7, 2024) [10.2514/6.2024-3184].

Availability:
This version is available at: 11583/2989659 since: 2024-06-18T14:54:49Z

Publisher:
AIAA

Published
DOI:10.2514/6.2024-3184

Terms of use:

This article is made available under terms and conditions as specified in the corresponding bibliographic description in the repository

Publisher copyright
AIAA preprint/submitted version e/o postprint/Author's Accepted Manuscript

(Article begins on next page)

18 November 2026

Sonic boom numerical validation of a Mach 4.7 experimental test

S.Graziani* , N.Viola.† and R.Fusaro ‡
Politecnico di Torino, Turin, Italy, 10129

Sebastien Hengy §, Marie Albisser ¶ and Bastien Martinez ‖
ISL, Saint Louis, France, 68300

This paper aims at validating the sonic boom numerical characterization obtained though CFD and a simple propagation methods against the results of an outdoor experimental test campaign for a future supersonic aircraft. Specifically, this paper investigates the sonic boom signature of a Mach 4.7 configuration, one of the case studies dealt with the EU-funded MORE&LESS project. The numerical approach reported in this paper consists in an extensive CFD simulation campaign carried out using the methodology proposed by NASA during the Sonic Boom Prediction Workshop held between 2014 and 2021, with a hybrid grid approach, consisted of a cylinder unstructured domain and a structured grid far from the geometry. Special treatment is given to the choice of the numerical scheme to be adopted during the simulations, as well to the aspect ratio and sonic glitch phenomenon. Complementary, the numerical results are compared to the experimental values gathered during Outdoor Sonic Boom Tests carried out in the open-field facility of ISL, properly equipped with acoustic measurement units.

Keywords: Sonic Boom, CFD, Experimental test

I. Nomenclature

dp/p	=	Increase in static pressure
H/L	=	Height to length ratio
C_L	=	Lift coefficient
C_D	=	Drag Coefficient
μ	=	Mach angle
θ	=	Misalignment angle
MORE&LESS	=	MDO and REgulations for Low-boom and
Environmentally Sustainable Supersonic Aviation	=	
CFD	=	Computational Fluid Dynamic
M	=	Mach number
p_s	=	Static Pressure
p_0	=	Free-stream pressure condition
RMS	=	Root Mean Square
α	=	Angle of attack, deg
ISA	=	International Standard Atmosphere
γ	=	ratio of specific heat
M_∞	=	Free-stream Mach number
y_0	=	Maximum value of $F(y)$
r	=	perpendicular distance from model to probe
ξ	=	apex half angle for the right circular cone
ρ	=	air density
a	=	speed of sound

*PhD Student, DIMEAS, samuele.graziani@polito.it
†full professor, DIGEP, nicole.viola@polito.it
‡assistant professor, DIMEAS, roberta.fusaro@polito.it
§Scientific Researcher, Sebastien.HENGY@isl.eu
¶Scientific Researcher, Marie.ALBISSER@isl.eu
‖Reserch Team Manager, Bastien.MARTINEZ@isl.eu

II. Introduction

The last decades have seen a renewed interest in the development of a new supersonic civil aircraft that could replace Concorde and enter into service in the near future [1]. All the efforts made have not yet led to the development of a civil aircraft due to both technical and environmental difficulties. One of the most critical and significant challenges in the development of a supersonic aircraft is the mitigation to acceptable levels of the noise generated by shock waves around the aircraft, which is technically called sonic boom.

Due to this phenomenon supersonic civil flights over the land are not allowed for the annoyance that caused to the population, and the ability to fly in supersonic regime everywhere is crucial to the economic success of future configurations. Since 1970s, numerous state-of-the-art study, technologies, and techniques have been developed to minimize sonic boom to fall within possible future imposed limits by regulatory authorities [2]. Those limits would be difficult to achieve by large configurations due to their requirements in terms of volume and lift. Nowadays, with the renewed interest in the development of a new generation of sustainable supersonic aircraft, there is an increasing activity in the study of new innovative concepts that can meet future sustainable requirements in terms of noise and pollutant emissions.

For the realisation of international standards defining the limits of sonic boom annoyance generated by supersonic aircraft, it is necessary to carry out numerous experimental tests both outdoors and indoors to determine the limit of human acceptability. In the last decade NASA, through the X-59 project [3] , has put huge effort in the development of a low-boom aircraft that can perform supersonic flights with a Mach number of 1.4 with a reduced annoyance to the population on the ground aiming for a sonic boom loudness of 75 dB in the metric of Stevens' MkVII Perceived Level of Noise [4] during cruise. The aircraft aims to be the reference for the definition of future international acceptability limits for supersonic flight over the land [5].

For the definition of future limits of acceptability, it is equally important to study psychoacoustic metrics that are capable of analysing human behaviour following stimuli of this kind in detail and experimental tests for sonic boom estimation are crucial. Firstly, they provide empirical data essential for understanding and mitigating the effects of sonic booms on structures and human. Secondly, they validate the results obtained by numerical simulations used to predict sonic boom. This process of experimentation and modeling not only aids in optimizing aircraft design to minimize sonic boom generation but also contributes to the formulation of robust regulatory frameworks. Thirdly help in refining aircraft design to minimize sonic boom intensity, thereby reducing its impact on communities.

The prediction of the sonic boom pressure variation is perceived on the ground by the population is a challenging task and requires the accurate prediction of the pressure signature generated by the aircraft in the supersonic regime. The study of the evolution of the signal from the aircraft at the reference altitude and the ground is usually divided in two main region as highlighted in Figure 1. In particular, the near-field region is the domain in the proximity of the aircraft where shock formation occurs and where non-linear phenomena are not negligible, such as shock-shock interactions, shock bending and cross flow and it usually evaluated using Computational Fluid Dynamics (CFD) with different numerical techniques validated.

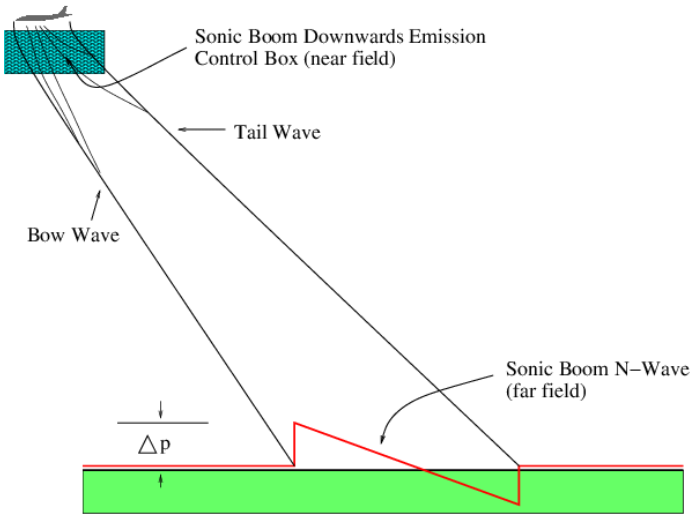


Fig. 1 Sonic boom Regions

The near-field pressure signature evaluated via CFD is propagated to the ground using propagation methods that are used in regions where the atmospheric variations and molecular relaxation are more important than the geometric details of the configuration. The accuracy of the propagation relies on the results of the near-field computation and it is influenced by other factors such as geometrical error due to surface mesh discretization, grid properties and viscosity. Yamashita and Suzuki [6] proposed another methodology to evaluate the sonic boom signature on the ground by using just computational fluid dynamics which took the domain from the cruising altitude to the ground, instead of using non linear equations for the far-field domain.
The following paper was carried out within the MORE&LESS project, that has the primary aim of investigating the environmental effects associated with supersonic aircraft operations. This investigation is conducted via multi-fidelity simulations and test campaigns to establish a comprehensive multidisciplinary framework that can be employed to assess the environmental impact of supersonic aircraft, their flight paths, and operational strategies. The project aims to analyze the flight regime between Mach 2 and 5 by evaluating different configurations and new propulsion technologies and assessing alternative fuels such as Biofuel and Liquid Hydrogen [7] [8] [9].
Within this paper, a series of sonic boom near-field simulations with different discretization methods were carried out to validate experimental test that were performed in 2023 and compared with the results given by the microphones. The remainder of this paper is organized as follows:

- In the first section, introduction and background are presented
- Section two highlights the case study, the methodology adopted for the realization of the simulations and experimental test setup
- Section three deals with the results obtained with the numerical simulations and the comparison with the experimental results
- Section four draws the conclusions and future works

III. Methodology

CFD techniques are used to study the near field region of a supersonic aircraft due to the strong non-linearities and three-dimensional interactions near the fuselage. In the vicinity of the aircraft, these turbulent effects dominate over the refraction effects of an inhomogeneous atmosphere, which will gain relevance in the subsequent far-field modelling.
Over the last two decades, numerous improvements were made in the study of sonic boom prediction [10] [11] [12] [13] in the near field. Since 2014, NASA has been promoting the AIAA Sonic Boom Prediction Workshop, which aims to define the numerical strategies and methodologies to accurately predict sonic booms. The computed pressure distribution of an aircraft is usually propagated further towards the ground using models which incorporate shock wave propagation in an inhomogeneous or even moving fluid. As well the Sonic Boom Prediction Workshop, a parallel Propagation Workshop was held to define the correct procedure for the propagation of the shock waves from the reference altitude to the ground.
The results of these two workshops represent the suggested approach for the definition and the propagation of shock waves surrounding the aircraft in supersonic regime from the reference free-stream condition at the operating altitude to the ground.

A. Case Study

The activities reported in this paper are part of the H2020 MORE&LESS project [14], MDO and REgulations for Low boom and Environmentally Sustainable Supersonic aviation), answering to the EC call "Towards global environmental regulation of supersonic aviation" (LC-MG-1-15-2020), aims at supporting Europe to shape global environmental regulations for future supersonic aviation [15]: recommendations are established on the basis of the outcomes of extensive high-fidelity modelling activities and test campaigns that merge into the multi-disciplinary optimization framework to assess the holistic impact of supersonic aviation onto environment. The reference concept analysed is a modified and scaled version of the Reaction Engine's Hypersonic Test Bed, that has a main driving requirement the SABRE flight demonstration and the de-risking of nacelle subsystems.
Main dimensions of the full scale configuration are reported in table 1, while the CAD of the model is reported in Figure 2.

Table 1 Characteristic of the full scale configuration

Characteristic	Dimension
Reference Surface $[m^2]$	40.77
Reference Length $[m]$	24.53
Center of Gravity position $[m]$	12.27
Wingspan $[m]$	8.67
Height $[m]$	3.81
Engine Diameter $[m]$	1.66
Fuselage Diameter $[m]$	1.902



Fig. 2 Full Configuration developed by REL

A re-design of the configuration reported in Figure 2 was necessary for the experimental test: firstly, the new configuration must not be subjected to stresses that would damage it during the free-flight experimental tests, and secondly it should not generate lift. A reinforcement was necessary to minimize deformations of body during launch, and due to high stress field in base region a risk of plastic deformation was resolved through the reinforcement of the projectile body.
The new configuration has been properly scaled to be suitable for the experimental test. The engine was removed due to construction constrain and the fin in the tail were increased in size due to stability purposes. Also for stability, the material of the nose of the aircraft is different compared to the body, in order to have a closer distances between center of gravity and center of pressure: the body is constructed with AL7075, while the nose with WNiFE(D176) and the total weight of the configuration is 437 grams.
The configuration was built with the aim of being stable in both planes, and a fixed static margin was used in the development of the aircraft to be on the safe side. The scaling law adopted for the mock up configuration is 1: 105, ensuring a total length just above 23 centimeters, and a picture of the mock up configuration used in the experimental test is highlighted in Figure 3. The main characteristics of the configuration used in the experimental test are reported in

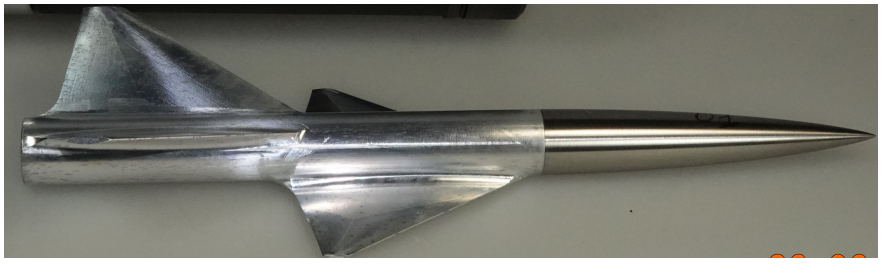


Fig. 3 Mock up Configuration used in the test

table 2 and the sketch is visible in Figure 4.

Table 2 Characteristic of the mock up configuration

Length $[cm]$	23.37
Weight $[kg]$	0.437
Center of gravity position $[cm]$	13.00
Wingspan $[cm]$	8.43
Fuselage diameter $[cm]$	0.81
Maximum Acceleration $[kg/s]$	35.0
Part in AL7075 $[cm]$	13.38

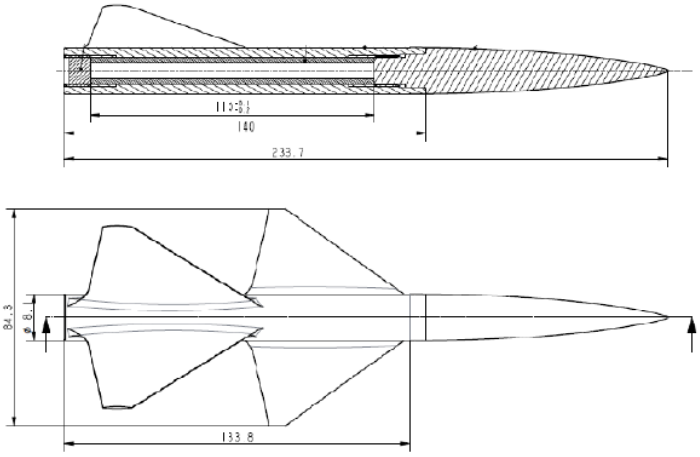


Fig. 4 Sketch of the Configuration

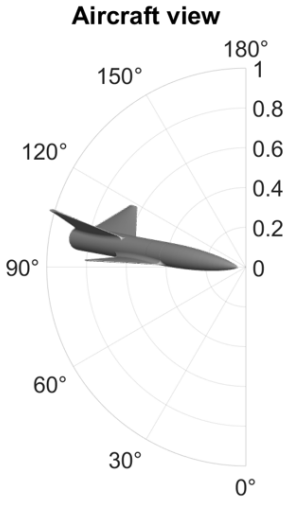


Fig. 5 Radial evaluation mock up mock up configuration

Figure 5 shows the radial evolution of the aircraft that will be used in the CFD extraction, with condition at 0° just below the configuration and 180° above it.
Several investigations are performed for a near-field assessment of the configuration: in particular, different numerical

schemes are tested to highlight differences in the signature at all extracted locations. The atmospheric conditions evaluated during the test campaigns were used in the simulations and reported in table 3.

Table 3 Atmospheric condition during tests

Condition	Value
Mach	4.7 []
Temperature	283 $[K]$
Pressure	98960 $[Pa]$
Wind	0 $[m/s]$
Humidity	83 [%]
a	337.92 $[m/s]$
ρ	1.2128 $[kg/m^3]$

The Euler equations, which account for mass and momentum balances excluding viscous effects, are numerically solved and integrated with a compressible perfect gas state model to close the entire system of equations.

B. CFD Approach & Computational domain

As already mentioned in the previous section, for the CFD simulations the approach used within this paper is the one promoted as a best practice during the AIAA Sonic Boom Prediction workshop.
The mesh strategy selection, in terms of refinement and adaptation approach allows the proper tracking of discontinuity needs specific effort. The topology of the computational grid follows a hybrid approach, composed by two different parts: an unstructured zone near the aircraft geometry and a structured one for the remaining domain of the grid much further from the geometry as highlighted in Figure 6. The unstructured part is designed as a cylinder in the domain, while the structured part is designed using a blocking technique and it is aligned with the Mach angle μ. The numerical elements are hexahedral in the structured domain, tetrahedral in the unstructured zone near the aircraft due to the very complex geometry, and pyramids to connect the two zones.
The advantages of this approach compared to the structured grid, is that the hybrid grid strategy preserve accuracy as well efficiency.

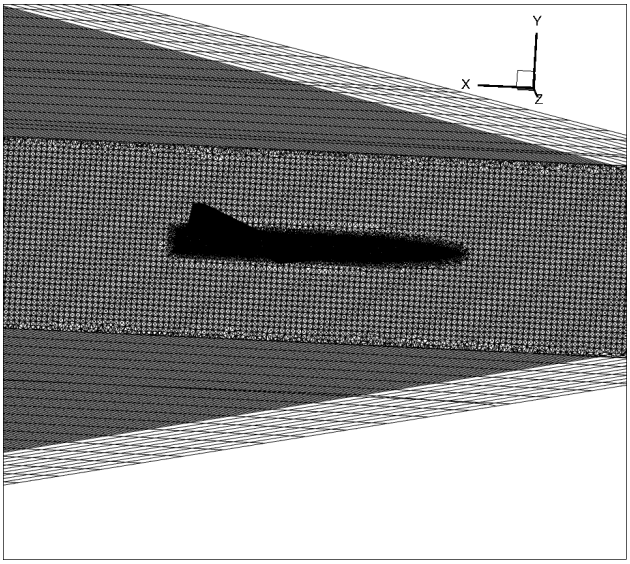


Fig. 6 Hybrid grid approach, particular of the difference between structured and unstructured domain

Previous work [16] have highlighted the importance of the alignment in the structured grid, especially for high displacement in the z direction, important differences in the signature were visible. Cartesian meshes can be effective in out-of-body signature computation as long as the mesh is aligned with the Mach angle μ of the free flow.
Good alignment reduces dissipative effects and the number of elements, so the signature can be computed to large distances over $H/L = 5$ without the necessity of long time for obtaining the convergences of the simulation. The H/L ratio is defined as the distances of extraction compared to the body length of the aircraft: the $H/L = 5$ is defined as a distance of extraction of 5 body length below the aircraft. However, a perfect alignment with the Mach angle μ could led to a numerical problem called sonic glitch phenomena that is avoided with a small misalignment $\mu \pm \theta$, with $\theta \ll \mu$. [17]

C. Computational Domain and grid generation

For the numerical aeroacoustic analyses of the mock up configuration due to the small dimension of the aircraft, even if it is axisymmetric it was decided to consider the full vehicle.
The free-stream conditions of the numerical simulation were the ones of the experimental test and previously reported in Table 3: the information of the Mach number was essential for the definition of the outer grid, since it is aligned to the Mach angle μ that is equal to 12.28°. To avoid the sonic glitch problem, the grid is not perfectly aligned with the angle μ, and for this particular case study it was adopted a misalignment of 0.32°, with an angle of the structured grid set to 12.6° as suggested by Anderson [18]. The domain of the simulation is visible in Figure 7.

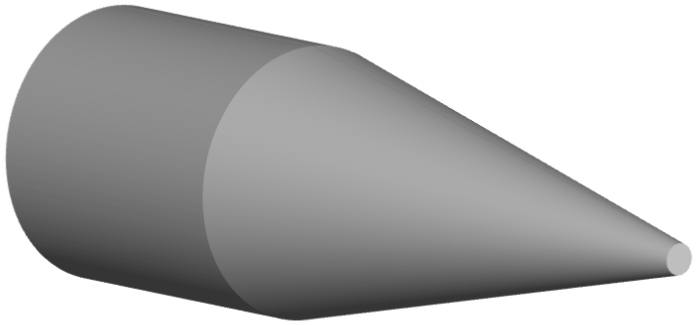


Fig. 7 Domain of the simulation

Due to the complexity of the geometry and very small thicknesses, an iterative cycle to define the degree of refinement of the aircraft was carried out as could be seen in Figures 8 and 9, with a total of surface elements along the mock up configuration of about 300000.
To capture shock waves effectively, special attention was paid to the definition of the simulation domain. In particular, it was decided to create a domain equal to one body length upstream of the aircraft and five body lengths downstream: in this way, it was possible to obtain accurate results and to capture at $H/L = 5$ the shock waves produced by the configuration without the necessity of high computational cost.
With this approach, the total number of elements are about 24 millions, with the unstructured domain that has about 13 millions of elements and the structured one with little below 10.
Regarding the aspect ratio of the computational elements, previous work carried out within the Second Sonic Boom Prediction Workshop [11] have highlighted that aspect ratio between 2 and 4 for all directions expect normal to the Mach wave improve the ratio between cost and accuracy.
Those studies show that higher aspect ratio could decrease the quality of the computed aerodynamic coefficient, even if they reduce considerably the number of cells for any test case, and in this analysis an important effort was put for having aspect ratio lower than 3.5.

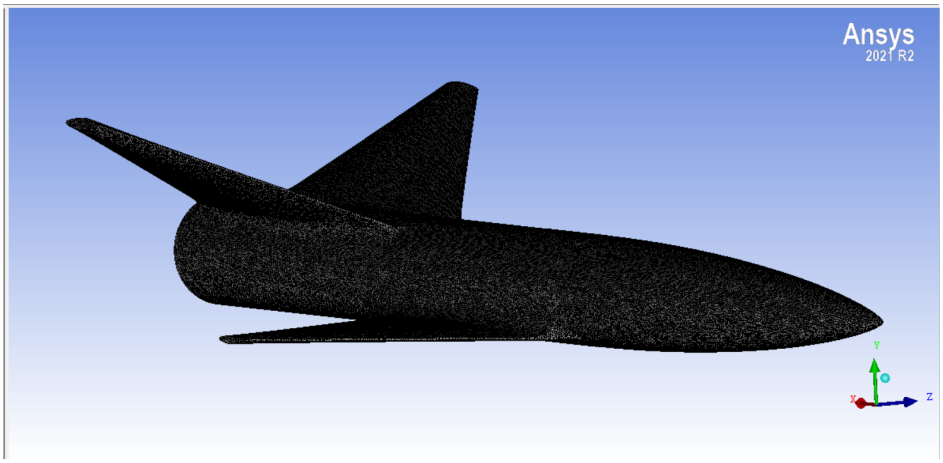


Fig. 8 Detail of the mesh in the aircraft

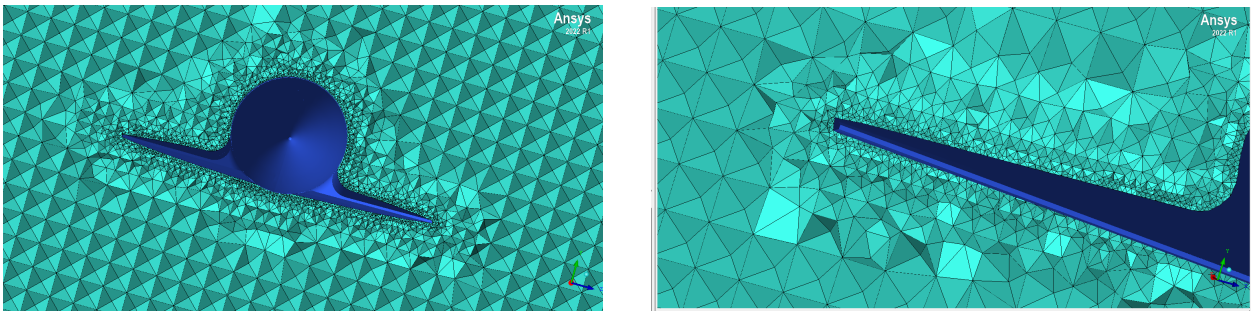


Fig. 9 Refinement within the aircraft surfaces, medium mesh

D. Setup and Solver

Near-field CFD simulations are conducted utilizing commercial Ansys Fluent [19] code. It emploies an unstructured finite-volume approach to solve the Reynolds-Averaged Navier-Stokes (RANS) equations on a hybrid grids, with gradients computed using a Green-Gauss method.

Fluent adopte an adaptive Courant-Friedrichs-Lewy (CFL) number as a convergence strategy, that adjust CFL values during simulation, optimizing stability and accuracy. Re-calibrating time-step sizes based on local flow conditions, Fluent ensures convergence across on local flow conditions. This adaptive approach ensure efficiency, enabling simulations to converge even with very complex fluid behaviors without any loss in the precision.

All simulations are carried out without turbulence models activated, solving inviscid Euler equations with an ideal gas model for the air.

Numerical schemes have a crucial role in the translation of equations from the continuous models to the discrete ones implemented in computational solvers. For the flight regimes analyzed in this paper, Fluent offers the second order upwind implicit ROE [20] [21] scheme with Flux-Difference Splitting ROE-FDS [22] based on the Roe scheme, which approximates a Riemann solver and it is particular useful for capturing discontinuity in the flows like shock waves.

Beside ROE-FDS scheme, Fluent also offers Advection Upstream Splitting Method (AUSM) that is a numerical method used to solve the advection equation.

The AUSM numerical scheme for Sonic Boom estimation has already been used in the past [23] [24] [25]. The peculiarity of the scheme lies in the decomposition of the flux vector into convective and pressure elements, a pivotal step in precisely managing phenomena like shock waves in fluid dynamics. Through the implementation of an upwinding strategy, the method computes fluxes at cell boundaries, facilitating accurate data transmission across the computational domain. An advantage of AUSM is its efficacy in handling strong shocks and sudden changes, areas where traditional methods often fail, resulting in instability or inaccuracies. AUSM dynamically adjusts these coefficients based on local flow conditions, ensuring stability and precision across diverse flow scenarios. It incorporates a flux-difference splitting approach, improving accuracy near discontiunities by considering both convenctive and pressure-gradient terms.

E. Experimental Setup

The experimental tests were carried out with one at ISL open range test site in Baldersheim, as a part of the MORE&LESS project.

The stability of the configuration was evaluated with both computational fluid dynamics and wind-tunnel tests. Also mechanical analysis such as Von Mises Stresses analysis were carried out to prevent from failure during the acceleration phase.

Four different tests were performed from a 91 mm smooth bore launcher, with an initial Mach number around 4.7, and a fire line of little more than 100 meters. The initial incidence of the configuration was 0° and a strong roll motion was observed during the tests due to the high position of the stabilisers.

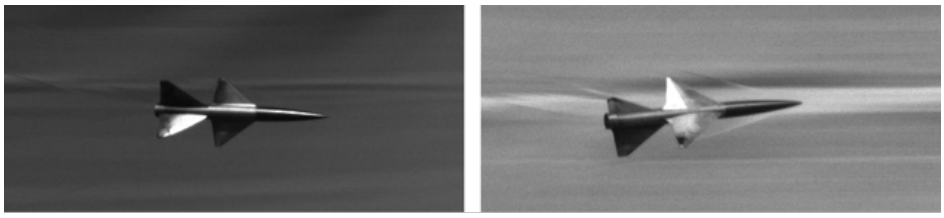


Fig. 10 Particular of the roll motion during the tests

As far as the measurement equipment is concerned, 15 ground microphones and two drone-supported microphones are deployed. The closest point of approach distance vary from 5 to 30 meters for all the deployed sensors. The measurements are undertaken on 15 ground positions down the range with ¼" Bruel&Kjaer microphones of type 4938. The setup of other components during the test consist of:

- Muzzle flash detector
- 10.5 Ghz radar
- Sky screens
- High speed cameras
- Sabot catcher

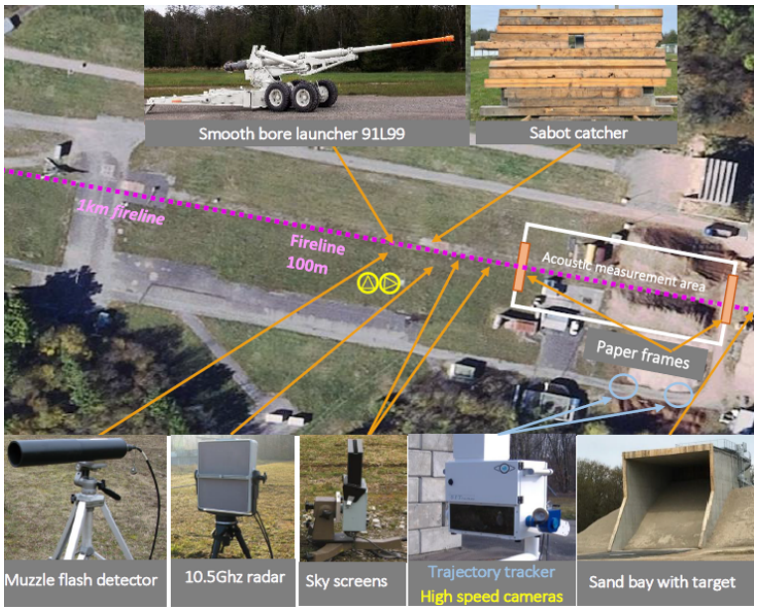


Fig. 11 Experimental Setup

During the field experiment, the microphones and drones have been deployed on the field in order to be able to observe the three dimensional propagation of the shock wave generated by the hypersonic projectile. Depending on the

flight attitude of the projectile, and according to Whitham's theory, the measured pressure and N-wave duration should vary as the influence of the projectile corpse and wings are different for each roll angle. This variation of the pressure and N-wave duration are expected to be observed on the measurements done with all the microphones deployed on the field.

In order to be able to analyze all the data correctly, the flight parameters of the projectile are measured at the entrance and at the exit of the measurement area for each of the four shots that have been fired. These results are visible in table 4.

Table 4 Flight parameters for the four recorded shots

Shot n°	V0(m/s)	M0	Vimpact(m/s)	Mimpact	Acc (G)	Pmax (bar)	Pmuzzle(bar)
1	1577	4.67	1540	4.56	35870	1100	89
2	1587	4.70	1549	4.58	36000	1100	90
3	1590	4.72	1553	4.61	35580	1092	95
4	1592	4.72	1543	4.57	36630	1120	95

F. Whitham Propagation Model

The theoretical model developed by Whitham provide a means to estimate the bow-shock sonic boom pressure rise at a specific distance. With the consideration of a steady, homogeneous, inviscid, supersonic flow over a slender body of revolution the flow perturbations can be expressed as integrals of the source distribution and can be related to a distribution of the body area:

$$F(y) = \frac{1}{2\pi} \int_0^y \frac{A"(x)}{\sqrt{y-\nu}} d\nu \tag{1}$$

In Equation 1, $A(x)$ is the cross-sectional area of the configuration as a function of the axial distance, ν is a variable of integration and y is the variable that identify the characteristic curve.
Using the Whitham's hypothesis on feature enhancement and applying his far-field at a sufficient distance from the body, such as the signature has evolved in the classical N-Wave, it is possible to obtain the relation evaluated in Equation 2:

$$\Delta P_s = \frac{2^{\frac{1}{4}} \gamma p_0 (M_\infty^2 - 1)^{\frac{1}{8}}}{(\gamma+1)^{\frac{1}{2}}} \sqrt{\int_0^{y_0} F(y) dy} \cdot r^{-\frac{3}{4}} \tag{2}$$

Due to the particular shape of the configuration to achieve an analytical formulation, a simpler shape was taken into account. Considering the case of a slender cone of finite length, the bow shock overpressure ΔP_s under the flight track could be calculated for an axisymmetric projectile in supersonic flight is just related to the geometry of the body and flight conditions as pointed out in Equation 3:

$$\Delta P_s = \frac{2^{\frac{1}{4}} \gamma p_0 (M_\infty - 1)^{(\frac{1}{8}}}{\sqrt{\gamma+1}} \left(\frac{4}{3} \xi^2 y_0^{\frac{3}{2}} \right)^{\frac{1}{2}} \cdot r^{-\frac{3}{4}} \tag{3}$$

The duration of the positive phase of the overpressure signature can be computed as in Equation 4.

$$\Delta y = \left(\frac{8}{3} k \xi^2 y_0^{\frac{3}{2}} \right)^{\frac{1}{2}} \cdot r^{\frac{1}{4}}$$

$$\Delta t = \frac{\Delta y}{M_\infty a} \tag{4}$$

IV. Results

Regarding the study of the sonic boom signature for this configuration, three main locations for the CFD extractions are: $H/L = 1$, $H/L = 3$, and $H/L = 5$. The choice of the number of cells plays a fundamental role in computational fluid dynamics for the trade-off between the convergence time of the simulations and the goodness of the results obtained and Advection upstream splitting Method is used. AUSM, was already validated for Sonic Boom simulations [23] [24]

[25].
Pressure and Mach number contour distribution around the mock up geometry in Figure 12 highlight the presence of existing shock waves.
The delta pressure distribution around the aircraft was evaluated with Equation 5:

$$dp/p = \frac{p_s - p_0}{p_0} \tag{5}$$

In Equation 5, p_s is the static pressure evaluated in the different locations and p_0 is the static free-stream pressure calculated during the test and equal to 98900 Pa.

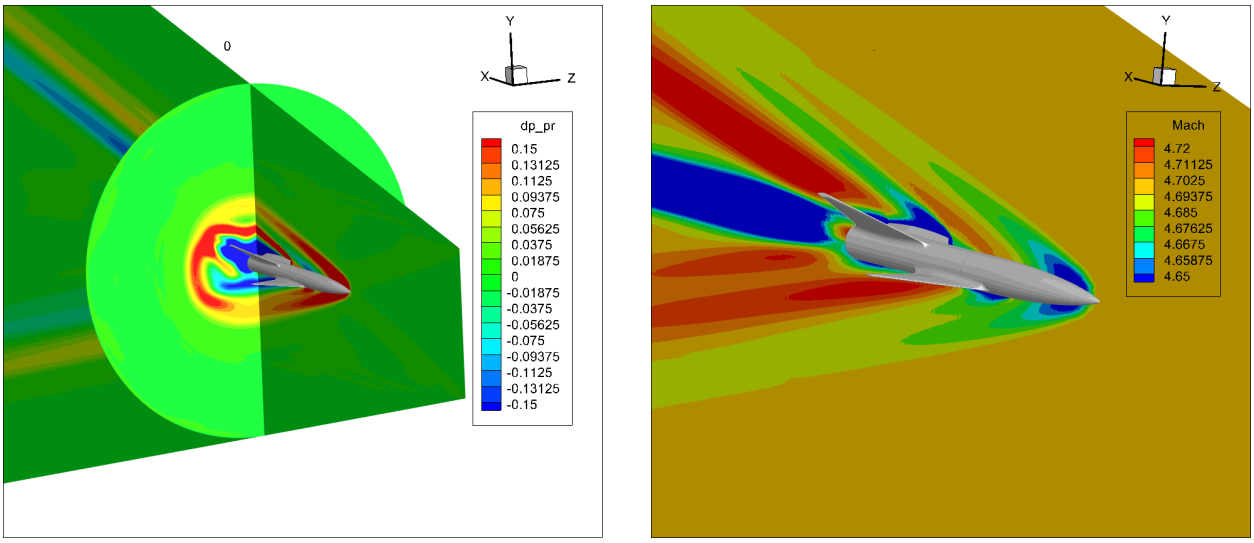


Fig. 12 Delta pressure and Mach number contour

Due to the shape of the aircraft, from the contour on the left hand side in Figure 12, it is possible to notice the immediate coalescence of shock waves of the nose and the wing, as this configuration was not studied with a design-to-noise approach.
The isolated contour of pressure distribution around the aircraft is highlighted in Figure 13, and it is pointed out the shocks interactions within the aircraft.

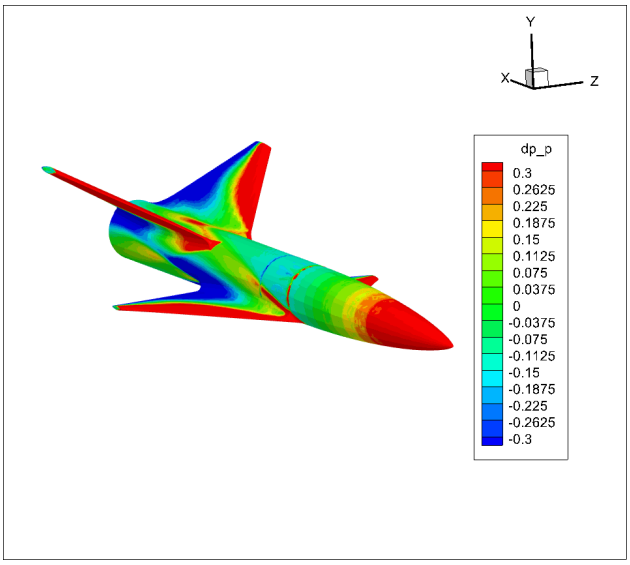


Fig. 13 Delta pressure contour, aircraft isolated

The pressure signature at $H/L = 3$ and $H/L = 5$ for the on-track condition are extracted, and there is not a particular difference in terms of the shape of the pressure signature, as could be highlighted in Figure 14, and as expected, the signature evaluated at $H/L = 5$ has a more linear trend due to the larger distances from the source.

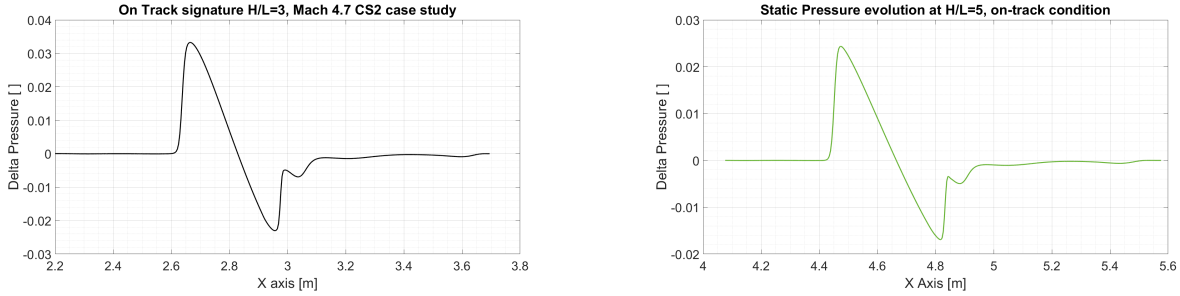


Fig. 14 Pressure Signature On-Track H/L=3,5

An acoustic radial analysis is carried out between 0° and 90° following the rule adopted in Figure 5 for the condition at $H/L = 3$: extraction were made every 15° to cover the aircraft. This is a result of a trade-off between a good radial evolution of the domain without the necessity of high computational power. It is possible to notice a marked difference in the evolution of the signature within different position of extraction for the expansion part as well, the value of peak pressure is slightly different between the points evaluated as could be seen in Figure 15.

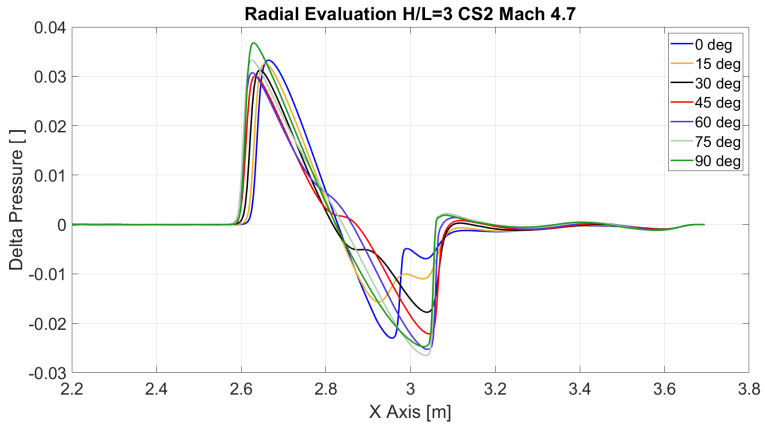


Fig. 15 Radial Evaluation, H/L=3

The same trend can be seen in the $H/L = 5$ radial evaluation, that is reported in Figure 16. As pointed out previously, there is a marked N-wave behaviour in the signature, due to high distance (i.e. H/L) and the coalescence of the shocks generated on the nose and the wing leading edge.

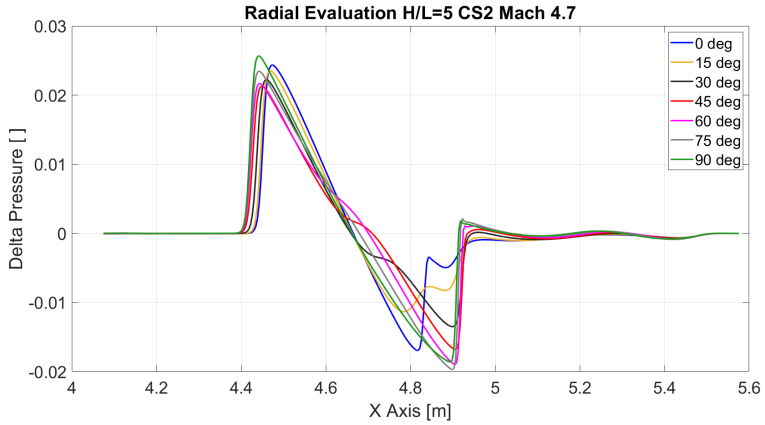


Fig. 16 Radial Evaluation, H/L=5

As visible from both Figure 15 and 16, there is a big difference between the peak value in compression and expansion. This is due to the particular geometry of the aircraft and to the dimensions of the stabilizer. The radial analysis was also carried out for radial extraction between 90° and 180° due to the axisymmetric geometry of the aircraft, and the results are highlighted in Figure 17. The maximum peak pressure is still located at 90° position, and for the following sections just the first 90 degrees were extracted.

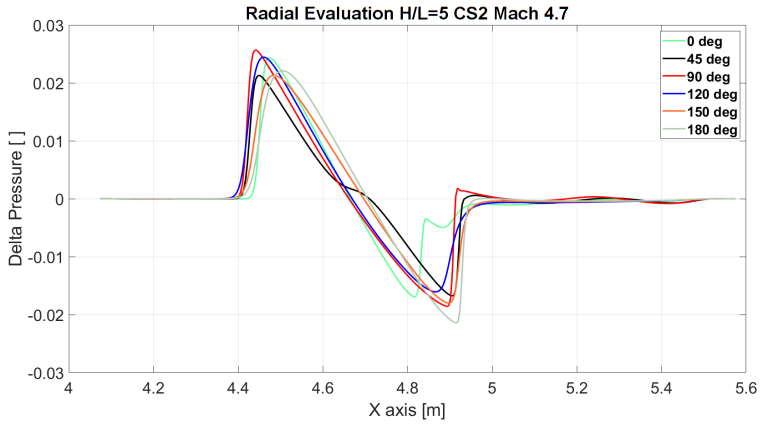


Fig. 17 Radial Evaluation for 180°, H/L=5

A. Sensitivity analysis with different numerical scheme

Firstly, a sensitivity analysis to numerical schemes for the mock up test case: comparing Computational Fluid Dynamics (CFD) simulations adopting different discretization method is a crucial work in numerical modelling. It helps understanding how different discretization methods affect results, identify errors, and boost confidence in outcomes. By doing so, it is possible to select the best scheme for each scenario, improving accuracy and saving time.
Additionally, the comparison of different numerical schemes helps to validate and identify which is the best discretization methods for sonic boom estimation.
Comparison between Advection Upstream Splitting Method (AUSM) and Roe scheme with Flux-Difference Splitting (ROE-FDS) was carried out for different position of extraction : the radial extraction was made for the 0°, 45° and 90° was made, and the results are showed in Figure 18.

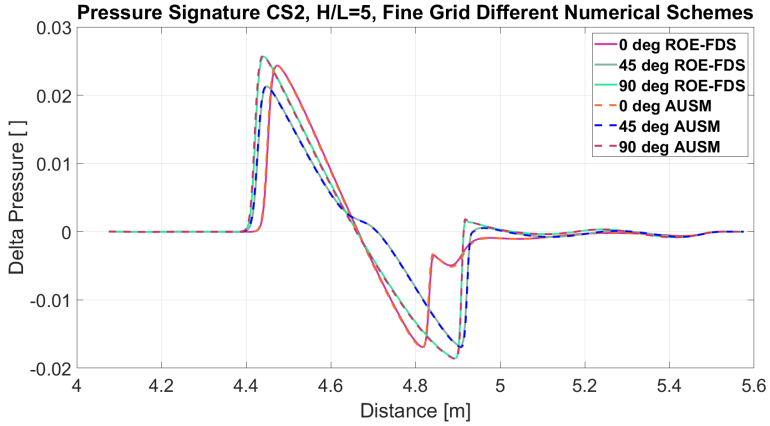


Fig. 18 Radial comparison for different numerical schemes

The results in Figure 18 highlight negligible differences between the two numerical schemes for the radial position evaluated at five body length of distance from the aircraft. The shape of the signature has the same trend for all the position evaluated, with minimal differences in the peak pressure. The same comparison was made for the $H/L = 3$ position extraction as could be seen in Figure 19.

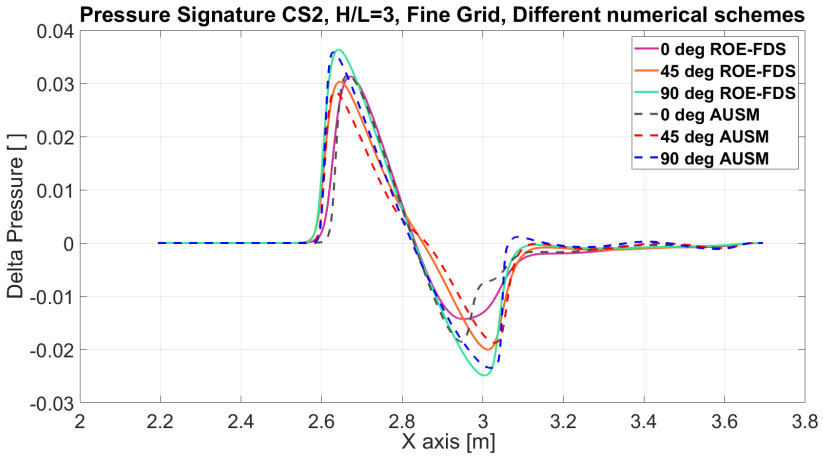


Fig. 19 Radial comparison for different numerical schemes, $H/L = 3$

Evaluating Figure 19, some slightly differences between the two discretization methods are visible, especially for the 45° condition. Compared to Figure 18, the shorter distance of extraction helps to show the differences within the pressure signature.

B. Experimental Results

During the field experiment, fifteen microphones have been deployed on the ground, at a 30 centimeters height, at five different cpa (closest point of approach) distances of 5, 10, 15, 20 and 30 meters on three lines at distances of 70, 85 and 100 meters from the 91 mm canon muzzle. The position of the sensors is measured with the help from a Real-Time Kinematik Global Positioning System. The sampling frequency of the 15 recorded signals is set to 192 kHz for each of the four small scale model firings as reported in Figure 20). For each microphone deployed during the firing, the duration of the N wave and the peak pressure in dB is measured.

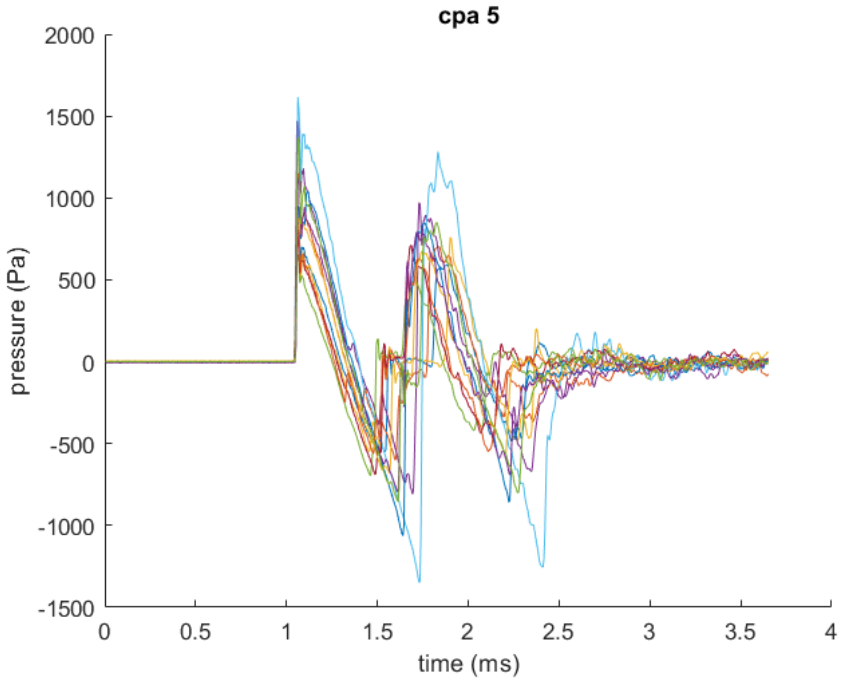


Fig. 20 Shock wave measured with the three microphones deployed at a 5 meters CPA for all shots

At cpa distances of 5, 10, 15, 20 and 30 meters, the large amount of measurements obtained with the ground microphones at these positions allows for the estimation of the mean observed N duration and peak pressure as showed in table 5. The mean values match the theoretical values obtained with Whitham's theory for an equivalent caliber of 30 millimeters. The estimated standard deviation at each cpa distance reaches a peak value of 167µs for the N-wave duration estimates, and a maximum +3.6dB peak value for the pressures estimates.

Table 5 mean peak pressure and shock wave duration

CPA $[m]$	5	10	15	20	30
mean duration $[\mu s]$	549.9	636.3	677.1	754.3	822.9
STD duration $[\mu s]$	83.3	104.6	105.6	130.6	167.6
mean peak pressure $[dB]$	154.0	149.7	147.1	146.2	143.1
STD peak pressure $[dB]$	2.6	3.6	2.1	2.1	2.2

In order to be able to compare the measured data and the CFD simulations results, it is necessary to propagate the CFD simulations from short range to long range propagation results. This process is described in the next section.

C. Numerical and Experimental results comparison

The results previously extracted via CFD are propagated at ranges equivalent to the ISL's microphones CPA. Therefore, propagation is carried out from the CFD extraction point to a distance of 30 metres, corresponding to the furthest positioning of the microphones.

Previous simulations at different extraction positions and different numerical schemes are aimed at identifying possible differences in the signature, and so differences in the comparison with ISL's results. Figure 21 highlights the comparison between CFD extracted at $H/L = 3$ with AUSM discretization method and propagated up to the intered cpa with the experimental tests. The range between 0 and 90 degrees was used since it is the area were the aircraft produce the maximum level of noise.

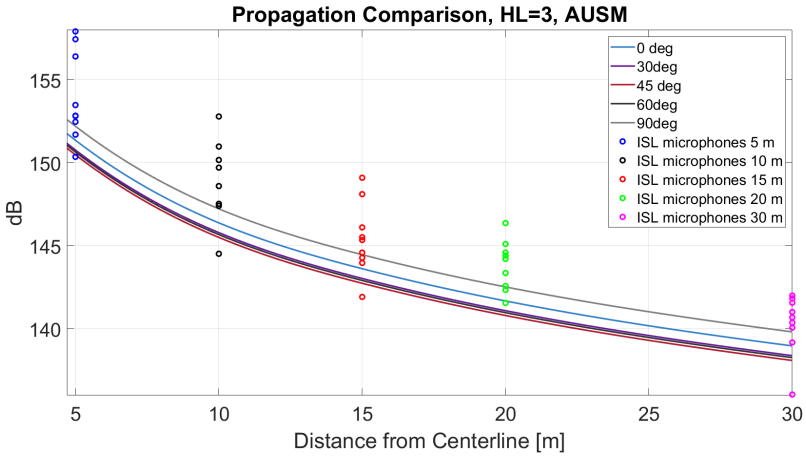


Fig. 21 Propagation from $H/L = 3$ results

The results obtained in Figure 21 highlight a similar trend for the propagation, especially in the first 15 meters. It is possible to identify some considerations between experimental results and CFD: in particular the first has a RMS much higher compared with the CFD, that is in the order of about 2 dB.

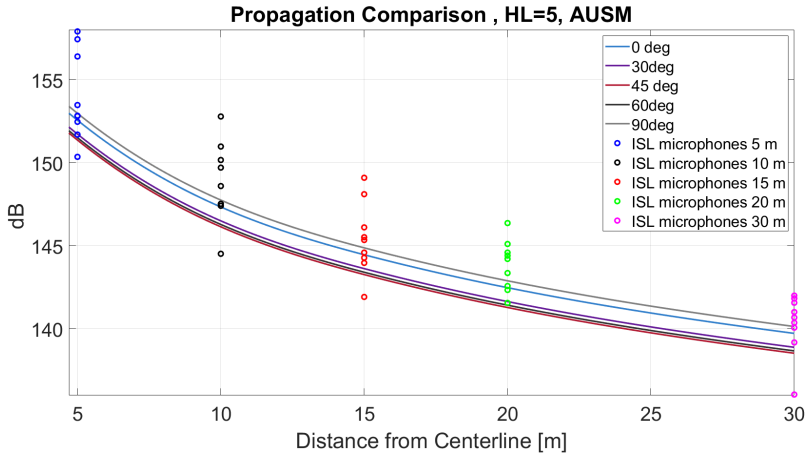


Fig. 22 Propagation from $H/L = 5$ results

The same results are highlighted in Figure 22 with the results of the CFD extracted at $H/L = 5$: the trend is the same of the previous comparison, with the CFD results that are within the experimental test domain. Comparing the CFD results of Figures 21 and 22 with the use of a simplified methodology for propagation, some slightly differences are visible within the two extraction point: in particular the maximum value of pressure is bigger with the $H/L = 5$ and the numerical RMS between every angle extraction is reduced.
The same approach was used to propagate results obtained with ROE-FDS method and the results are visible in Figure 23 and 24.

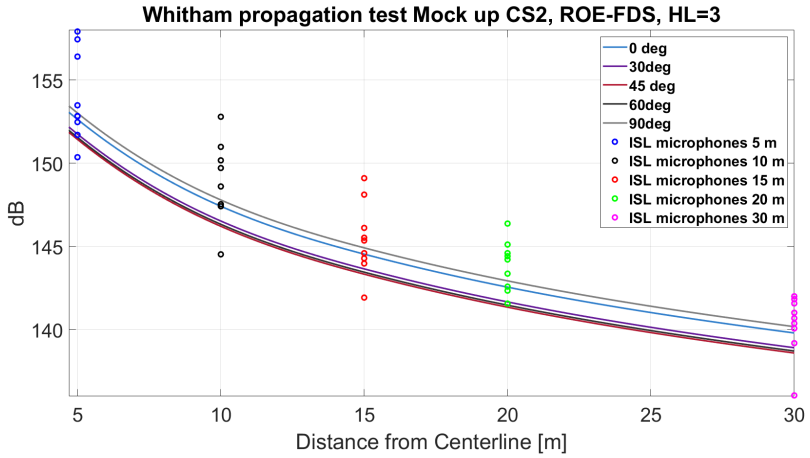


Fig. 23 Propagation from $H/L = 3$ results, ROE-FDS

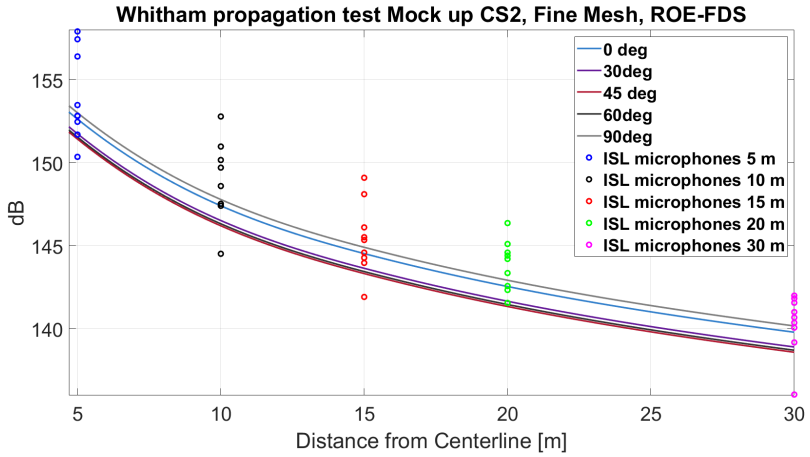


Fig. 24 Propagation from $H/L = 5$ results, ROE-FDS

The results highlighted in Figure 23 and 24 are similar to the ones highlighted with the Advection Upstream Splitting Method (AUSM): the behaviour with the two different discretization methods is the same, and also the value in peak pressure at every distance covered is similar for both $H/L = 3$ and $H/L = 5$.
The experimental tests are within the value given by the CFD, and the same consideration of the numerical RMS could be exploited for ROE-FDS numerical scheme.

V. Conclusion

This paper aims at validating the sonic boom numerical characterization obtained through CFD and simple propagation methods against the results of an outdoor experimental campaign for a future supersonic aircraft. Numerically, particular attention was given to the construction of the numerical grid, with a small misalignment in the structured domain of about 0.3° to avoid the sonic glitch phenomenon, and also maximum aspect ratio was evaluated.
Different numerical schemes were adopted in these simulations, in particular the Advection Upstream Splitting Method (AUSM) already validated for sonic boom analysis and ROE-FDS were used: negligible differences are visible within the signature for larger distances of extraction.
The results given by the CFD were propagated to the ground at the ISL's microphones, with a distance between 5 to 30 meters from the centerline. The propagation was carried out using a simplification within the Whitham theory and considering the configuration as a projectile. Some loss of accuracy is visible from distances up to 15 meters, while for the first part of the extraction the results are in line with the experimental test. The experimental test show a higher RMS between the values obtained in the microphones, and this is due to the strong roll motion of the aircraft that can coalescence the shock waves emitted by the aircraft.
Future works will assess the differences given by different grids, investigating the accuracy of much coarser meshes with limited computational cost. A relation between full-scale and mock up aircraft is on-going and finally, the use of open-source software's will be investigated as well.

Acknowledgments

Authors would like to thank all the partners of MORE&LESS project.

References

[1] Liebhardt, B., and Lütjens, K., "An Analysis of the Market Environment for Supersonic Business Jets," 2011.

[2] Sun, Y., and Smith, H., "Review and prospect of supersonic business jet design," *Progress in Aerospace Sciences*, Vol. 90, 2017, pp. 12–38. https://doi.org/https://doi.org/10.1016/j.paerosci.2016.12.003.

[3] Rathsam, J., Coen, P., Loubeau, A., Ozoroski, L., and Shah, G., "Scope and goals of NASA's Quesst Community Test Campaign with the X-59 aircraft," *14th ICBEN Congress on Noise as a Public Health Problem*, 2023.

[4] Stevens, S. S., "Perceived Level of Noise by Mark VII and Decibels (E)," *The Journal of the Acoustical Society of America*, Vol. 51, No. 2B, 1972, pp. 575–601. https://doi.org/10.1121/1.1912880, URL https://doi.org/10.1121/1.1912880.

[5] Doebler W., L. A., Wilson S., and V., S., "Five-year simulation study of NASA X-59 low-boom carpets across the contiguous United States of America," *eForum Acusticum 2020*, 2020, pp. 1001–1008.

[6] Yamashita, R., Makino, Y., and Roe, P. L., "Fast Full-Field Simulation of Sonic Boom Using a Space Marching Method," *AIAA Journal*, Vol. 60, No. 7, 2022, pp. 4103–4112. https://doi.org/10.2514/1.J061363.

[7] Roncioni, P., Marini, M., Gori, O., Fusaro, R., and Viola, N., "Aerodatabase Development and Integration and Mission Analysis of a Mach 2 Supersonic Civil Aircraft," *Aerospace*, Vol. 11, 2024, p. 111. https://doi.org/10.3390/aerospace11020111.

[8] Viola, N., Fusaro, R. A., Saracoglu, B. H., Schram, C., Grewe, V., Martínez, J. A. R., Marini, M., Hernández, S., Lammers, K., Vincent, A., Hauglustaine, D., Liebhardt, B., Linke, F., and Fureby, C., "Main Challenges and Goals of the H2020 STRATOFLY Project," *Aerotecnica Missili & Spazio*, Vol. 100, 2021, pp. 95 – 110. URL https://api.semanticscholar.org/CorpusID:236394667.

[9] Graziani, S., Viola, N., Petrosino, F., and Jäschke, J., *Comparison between simplified approach and CFD & Propagation tool for sonic boom estimation*, ???? https://doi.org/10.2514/6.2023-4166.

[10] Park, M. A., Aftosmis, M. J., Campbell, R. L., Carter, M. B., Cliff, S. E., and Bangert, L. S., "Summary of the 2008 NASA Fundamental Aeronautics Program Sonic Boom Prediction Workshop," *Journal of Aircraft*, Vol. 51, No. 3, 2014, pp. 987–1001. https://doi.org/10.2514/1.C032589.

[11] Park, M. A., and Morgenstern, J. M., "Summary and Statistical Analysis of the First AIAA Sonic Boom Prediction Workshop," *Journal of Aircraft*, Vol. 53, No. 2, 2016, pp. 578–598. https://doi.org/10.2514/1.C033449.

[12] Park, M. A., and Nemec, M., "Nearfield Summary and Statistical Analysis of the Second AIAA Sonic Boom Prediction Workshop," *Journal of Aircraft*, Vol. 56, No. 3, 2019, pp. 851–875. https://doi.org/10.2514/1.C034866.

[13] Park, M. A., and Carter, M. B., *Nearfield Summary and Analysis of the Third AIAA Sonic Boom Prediction Workshop C608 Low Boom Demonstrator*, ???? https://doi.org/10.2514/6.2021-0345.

[14] Horizon2020, "MDO and REgulations for Low-boom and Environmentally Sustainable Supersonic aviation," *Grant agreement ID: 101006856*, 2021. https://doi.org/https://doi.org/10.3030/101006856.

[15] Piccirillo, G., Graziani, S., Fusaro, R., and Viola, N., "LTO NOISE AND SONIC BOOM PREDICTIONS IN EARLY CONCEPTUAL DESIGN PHASES," 2022.

[16] Park, M. A., Campbell, R. L., Elmiligui, A. A., Cliff, S. E., and Nayani, S., *Specialized CFD Grid Generation Methods for Near-Field Sonic Boom Prediction*, ???? https://doi.org/10.2514/6.2014-0115.

[17] Moschetta, J.-M., and Gressier, J., *The sonic point glitch problem: A numerical solution*, 2007, pp. 403–408. https://doi.org/10.1007/BFb0106615.

[18] Anderson, G. R., Aftosmis, M. J., and Nemec, M., "Cart3D Simulations for the Second AIAA Sonic Boom Prediction Workshop," *Journal of Aircraft*, Vol. 56, No. 3, 2019, pp. 896–911. https://doi.org/10.2514/1.C034842.

[19] *Ansys Fluent Fluid Simulation Software*, release 18.1 ed., ANSYS, Inc., 2018.

[20] Roe, P., "Approximate Riemann solvers, parameter vectors, and difference schemes," *Journal of Computational Physics*, Vol. 43, No. 2, 1981, pp. 357–372. https://doi.org/https://doi.org/10.1016/0021-9991(81)90128-5.

[21] Roe, P., "Approximate Riemann solvers, parameter vectors, and difference schemes," *Journal of Computational Physics*, Vol. 43, No. 2, 1981, pp. 357–372. https://doi.org/https://doi.org/10.1016/0021-9991(81)90128-5, URL https://www.sciencedirect.com/science/article/pii/0021999181901285.

[22] Roe, P. L., "Characteristic-Based Schemes for the Euler Equations," *Annual Review of Fluid Mechanics*, Vol. 18, No. 1, 1986, pp. 337–365. https://doi.org/10.1146/annurev.fl.18.010186.002005.

[23] Wintzer, M., Nemec, M., and Aftosmis, M., *Adjoint-Based Adaptive Mesh Refinement for Sonic Boom Prediction*, ???? https://doi.org/10.2514/6.2008-6593.

[24] Dagrau, F., Loseille, A., and Din, I. S. E., *Computational and Experimental Assessment of Models for the First AIAA Sonic Boom Prediction Workshop Using Adaptive High Fidelity CFD methods*, ???? https://doi.org/10.2514/6.2014-2009.

[25] Luquet, D., Marchiano, R., Coulouvrat, F., Din, I. S. E., and Loseille, A., *Sonic Boom Assessment of a Hypersonic Transport Vehicle with Advanced Numerical Methods*, ???? https://doi.org/10.2514/6.2015-2685.